ACS APPLIED ENGINEERING MATERIALS

pubs.acs.org/acsaenm Article

Toughening Polymer-Derived Ceramics with Boron Nitride Nanotubes

Nasim Anjum, Dingli Wang, and Changhong Ke*

Cite This: ACS Appl. Eng. Mater. 2025, 3, 2383−2390 Read Online

ACCESS | Metrics & More | Article Recommendations | Supporting Information

ABSTRACT: We report the mechanical reinforcement of polymer-derived silicon oxycarbide (SiOC) through incorporating boron nitride nanotubes (BNNTs). Adding small amounts of BNNTs (up to 1.0 wt %) in SiOC precursors results in a remarkable 2.5-fold increase in flexural strength and a 3.3-fold increase in fracture toughness. The study reveals a brittle-to-ductile transition in BNNT-SiOC nanocomposites, increasing the deformability of the SiOC matrix. The introduction of small amounts of BNNTs noticeably reduces matrix porosity and promotes appreciable increases in matrix crystallinity. The findings demonstrate the potential of BNNTs as effective reinforcing fillers in polymer-derived ceramics, opening avenues for developing lightweight, high-strength, tough, and durable ceramic materials.

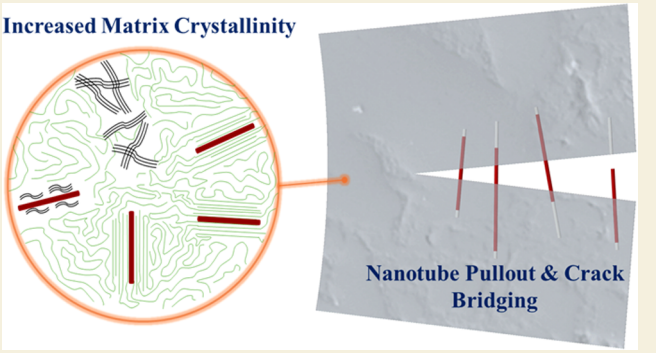

KEYWORDS: *boron nitride nanotubes, polymer-derived ceramics, ceramic matrix composites, mechanical enhancement, microstructures*

1. INTRODUCTION

Polymer-derived ceramics (PDCs) constitute a distinctive class of ceramics characterized by their superior manufacturability, enabling a broad range of applications across industries, such as aerospace, energy, and biomedical sectors.[1] In contrast to conventional ceramics, which are fabricated via glass or particulate forming followed by sintering, PDCs are synthesized via a polymer-to-ceramic transformation—typically through thermal decomposition and densification in an inert atmosphere—offering enhanced malleability for shape-forming. However, pyrolysis-driven volatilization of organic constituents results in inherently porous microstructures, which significantly compromise mechanical integrity and render PDCs susceptible to fracture, a long-standing shortcoming for ceramics. Filler-based reinforcement strategies have been explored to enhance the bulk mechanical properties of PDCs. Notably, recent studies report a 3-fold increase in the fracture toughness of polymer-derived silicon oxycarbide (SiOC) reinforced with microparticles (diamond, ∼1.2 μm, 20 vol %)[2] and nanoparticles (aluminum silicate, ∼700 nm, 35 vol %).[3] Despite these enhancements, the relatively high filler loadings (20−35 vol %)—comparable to those used in traditional ceramic matrix composites—indicate only moderate reinforcement efficiency on a per-unit-filler-percentage basis.

Boron nitride nanotubes (BNNTs) have emerged as a highly promising nanofiller for reinforcing PDCs, owing to their low density, high surface area-to-volume ratio, and exceptional intrinsic properties—most notably a Young's modulus approaching ∼1.3 TPa and tensile strengths up to ∼60 GPa.[4−6] BNNTs also exhibit remarkable thermal stability, remaining stable up to ∼900 °C in air[7] and exceeding 1800 °C in inert atmospheres.[8] The partially ionic nature of B−N bonds creates a rugged and anisotropic energy landscape at the ceramic binding interface, leading to enhanced shear resistance with nanotube pullout as the dominant interfacial failure mechanism.[9,10] The interfacial behavior enables BNNTs to function as nanoscale crack arresters and to facilitate energy dissipation through frictional sliding during nanotube pullout events. Additionally, BNNTs act as nucleation sites during high-temperature pyrolysis, facilitating phase transformations and crystallization within the ceramic matrix, thereby contributing to enhanced structural integrity and improved mechanical performance.[11,12]

To date, investigations into the reinforcement of PDCs using BNNTs remain scarce. The few studies on BNNT-PDC nanocomposites have primarily focused on thermal properties, employing relatively high BNNT loadings—for instance, ∼35 vol % as reported by Jia et al.[13] and ∼10−80 wt % by Li et al.[14] While such high concentrations enhance thermal conductivity and stability, they inevitably introduce nonidealities such as nanotube aggregation, bundling, and network formation.

Received: April 23, 2025
Revised: July 16, 2025
Accepted: July 16, 2025
Published: July 21, 2025

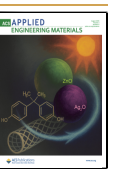

https://doi.org/10.1021/acsaenm.5c00295
ACS Appl. Eng. Mater. 2025, 3, 2383−2390

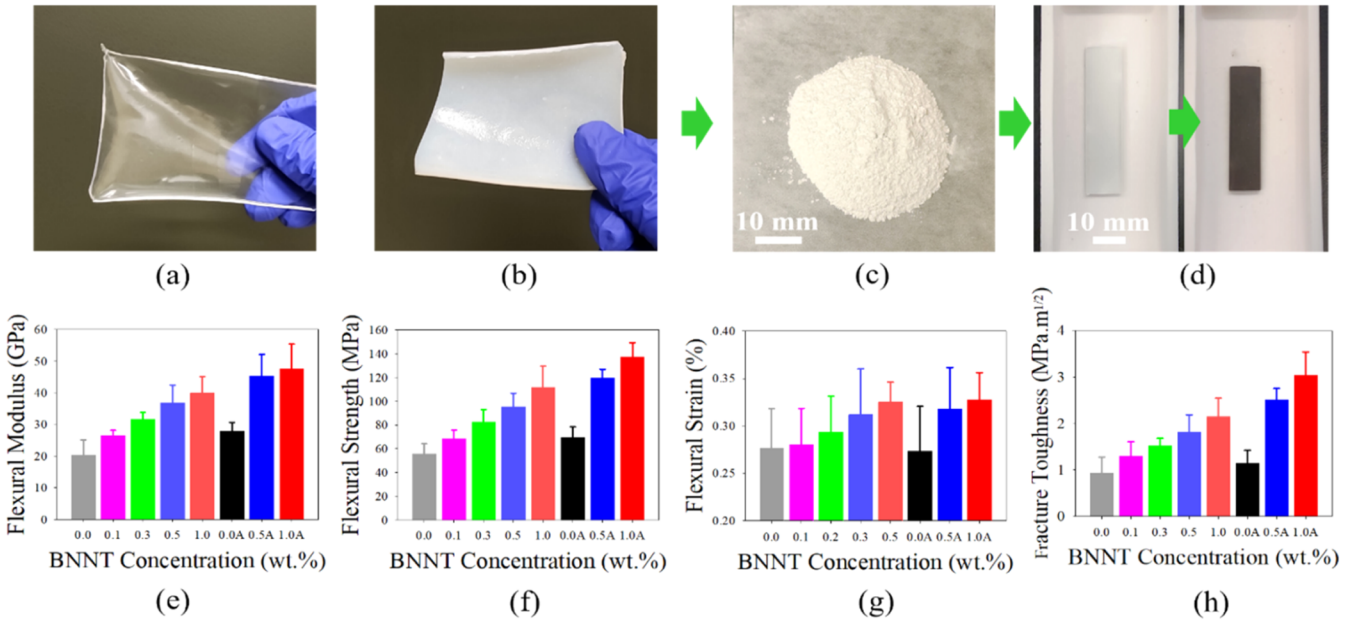

Figure 1. Manufacturing and mechanical characterization of BNNT-SiOC nanocomposites: cross-linked films of (a) pure H44 and (b) 0.5% BNNT-H44; (c) White powder after crushing and ball milling of BNNT-H44 film in (b); (d) Pyrolysis of white BNNT-H44 composite bar into black bar at 1000 °C; (e−h) The measured flexural modulus, strength and strain, and fracture toughness of thermally pyrolyzed and annealed BNNT-SiOC. The suffix A in BNNT concentration refers to annealed specimens.

Those structural defects can compromise dispersion uniformity and interfacial bonding, ultimately diminishing the reinforcement efficiency of BNNTs or degrading the composite's bulk mechanical properties.[14]

In this study, we investigate the mechanical reinforcement of polymer-derived SiOC through incorporating small amounts of BNNTs (up to 1.0 wt %). Our results show that BNNT addition leads to significant multifold increases in flexural strength and fracture toughness, along with a markedly improved deformability. The property enhancements are attributed to efficient load transfer at the nanotube−matrix interface and favorable microstructural modifications induced by BNNTs, including reduced porosity and improved crystallinity.

2. MATERIALS AND METHODS

2.1. BNNTs and PDCs

BNNTs used in this study were purchased from BNNT Materials, Inc., with a BNNT purity of ∼88% and BN purity exceeding 99%.[11] These tubular BN nanostructures, synthesized using high-temperature pressure (HTP) methods, exhibit high crystallinity, with very few tube walls (mostly 1−4 walls), small diameters, and lengths reaching up to several hundred microns.[15] Prior studies indicate that HTP-BNNTs are predominantly double-walled structures with a mean diameter of about 2.9 nm.[16,17] A commercial preceramic resin H44 (Jen-Tek Industries, LLC) is used in this study. When pyrolyzed in an inert atmosphere, H44 converts into a SiOC ceramic matrix with a silicon oxide content of ∼82%, according to the manufacturer.

2.2. Thermal Processing

The thermal curing process of the white BNNT-PDC specimen is conducted inside a tube furnace in three stages: (1) heating from room temperature to 250 °C at a rate of 4 °C/min, followed by a 30 min hold; (2) further heating to 700 °C at a rate of 1.1 °C/min, followed by a 20 min hold; (3) further heating to 1000 °C at a rate of 1 °C/min, followed by a 2-h hold. The thermal annealing process of the pyrolyzed BNNT-PDC specimen is conducted inside the same tube furnace in two stages: (1) heating from room temperature to 250 °C at a rate of 4 °C/min, followed by a 30 min hold; (2) further heating to 1400 °C at a rate of 3 °C/min, followed by varying hold time (up to 5 h).

2.3. Mechanical Characterization

The flexural and fracture toughness properties of BNNT-PDC nanocomposites were evaluated using quasi-static three-point bending tests: (i) unnotched specimen (Figure S1a in the in the Supporting Information) for flexural strength measurements with nominal dimensions of length ∼14.5 ± 0.5 mm, depth ∼3.9 ± 0.1 mm, thickness ∼1.25 ± 0.1 mm; (ii) single-edge notched specimen (Figure S1b) for fracture toughness measurements with nominal dimensions of length ∼17.5 ± 0.5 mm, depth ∼4 ± 0.1 mm, thickness ∼1.8 ± 0.1 mm, notch length ∼2 ± 0.1 mm, and notch root radius ∼0.3 ± 0.05 mm. Both types of specimens were characterized inside a mechanical tester (ADMET) at a loading rate of 0.2 mm/min. At least five different samples were mechanically characterized for each type of nanocomposite specimen. The flexural modulus and fracture toughness are analyzed using the approaches reported in our recent work.[11,18] Unless otherwise specified, all reported mechanical measurement results regarding the annealed specimens were annealed at 1400 °C for 3 h (Figure S2).

2.4. Material Characterization

Thermogravimetric analysis (TGA) was performed using Netzsch Thermogravimetric Analyzer, TG 209 F1. Raman micromechanical measurements were performed in situ using a Linkam TST350 mechanical tester integrated with a Renishaw inVia Raman microscope (532 nm laser and 50× objective lens). Scanning electron microscopy (SEM) and energy-dispersive X-ray spectroscopy (EDS) measurements were conducted using a Zeiss Supra 55 field-emission SEM. X-ray diffraction (XRD) measurements were conducted using a Panalytical X-ray Diffractometer

2.5. Finite Element Simulations

A 3D finite element model was established to simulate the local strain in the notched BNNT-PDC nanocomposite specimen under the three-point bending test using commercial code ANSYS. By assuming isotropy and homogeneity of BNNT-PDC nanocomposite specimens, three-dimensional volume elements "SOLID185" with eight nodes and three degrees of freedom per node were used in the simulations.

https://doi.org/10.1021/acsaenm.5c00295
ACS Appl. Eng. Mater. 2025, 3, 2383−2390

Table 1. Summary of the Measured Structural and Mechanical Properties of BNNT-SiOC Nanocomposites (Suffix A in BNNT Concentration Refers to Annealed Specimens)

BNNT concentrations (%)	density (g/cm^3)	flexural modulus (GPa)	flexural strength (MPa)	flexural strain (%)	fracture toughness (MPa·m$^{1/2}$)
0.0	1.97 ± 0.02	20.4 ± 4.7	55.5 ± 9.0	0.27 ± 0.04	0.9 ± 0.4
0.0A	2.17 ± 0.04	29.9 ± 2.8	69.3 ± 9.2	0.28 ± 0.03	1.1 ± 0.3
0.1	1.97 ± 0.02	26.6 ± 1.6	68.4 ± 7.4	0.29 ± 0.03	1.3 ± 0.3
0.3	1.99 ± 0.03	31.7 ± 2.1	82.8 ± 10.2	0.31 ± 0.05	1.5 ± 0.2
0.5	2.00 ± 0.03	36.8 ± 5.7	95.6 ± 11.2	0.32 ± 0.02	1.8 ± 0.4
0.5A	2.20 ± 0.02	45.4 ± 6.8	119.6 ± 7.4	0.27 ± 0.05	2.5 ± 0.3
1.0	2.03 ± 0.01	40.0 ± 5.3	111.6 ± 18.2	0.32 ± 0.04	2.2 ± 0.4
1.0A	2.20 ± 0.02	47.6 ± 7.9	137.4 ± 11.9	0.33 ± 0.03	3.0 ± 0.5

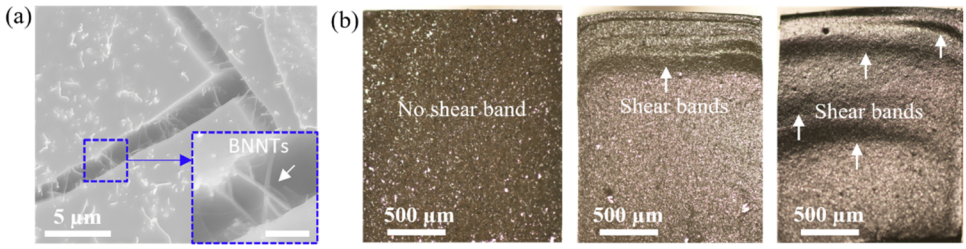

Figure 2. Surface morphology of fractured BNNT-SiOC nanocomposites: (a) SEM image showing protruding BNNTs from the fractured surface that bridge across load-induced microcracks (inset scale bar 1 μm); (b) Optical images of fractured surface of pure SiOC (*left*), 1.0% pyrolyzed BNNT-SiOC (*middle*), and annealed 1.0% BNNT-SiOC (*right*).

3. RESULTS AND DISCUSSION

3.1. Manufacturing and Mechanical Characterization

To fabricate pure PDC specimens, H44 resin is dissolved at a mass ratio of 23% in a solvent mixture of dimethylformamide (DMF) and acetone (7:3 ratio). The solution is agitated using a shaker until the resin is fully dissolved. A thin film is then cast and air-dried at 70 °C for 12 h. The dried film is subsequently cross-linked at 250 °C for 1 h, yielding a transparent, cross-linked H44 polymer film (Figure 1a). To manufacture BNNT-reinforced PDC specimens, as-received BNNTs are first dispersed in the same DMF/acetone mixture using bath sonication (1 h per 0.1% weight concentration). Then, H44 resin powder is added to the BNNT suspension. The resulting mixture is dried and then cross-linked, forming a white, solid composite material (Figure 1b). It is subsequently crushed, ground, and sieved through a 50 μm mesh. The produced fine composite powders (Figure 1c) are pressed into rectangular bars (50 mm × 12 mm × 2.5 mm) under a pressure of 5000 lbs at 250 °C for 10 min using a 15-ton Carver hot press. The white BNNT-PDC bars are then thermally pyrolyzed at 1000 °C (referred to as *pyrolyzed specimens*), with selected specimens further annealed at 1400 °C (*annealed specimens*) in a nitrogen atmosphere inside a tube furnace.

BNNT−PDC specimens are fabricated with nominal BNNT concentrations of up to 1 wt %, calculated as the weight ratio of BNNTs to preceramic resins. Unless otherwise specified, BNNT concentrations are reported as weight percentages throughout this study. As shown in Figure 1d, pyrolysis at 1000 °C results in ∼22.5% shrinkage and a color change from white to black, attributed to the formation of free carbon.[19] Additional annealing at 1400 °C for 3 h induces further shrinkage, yielding a total size reduction of ∼30% relative to the original. EDS analysis confirms a uniform distribution of BNNTs (1%) within SiOC (Figure S3), indicating that the processing of PDCs facilitates the effective incorporation of BNNTs. In contrast, conventional ceramics—particularly those fabricated using particle-based slurry methods (such as silica[11])—often exhibit microstructural heterogeneity, such as nonuniform BNNT dispersion.

For both pyrolyzed and annealed BNNT-SiOC, mechanical property improvements increase with BNNT concentration, and annealed specimens consistently outperform their pyrolyzed counterparts with the same BNNT loading. For instance, incorporating 1% BNNTs increases the flexural modulus of pyrolyzed SiOC by ∼96% from ∼20.4 to ∼40.0 GPa. Thermal annealing alone improves the flexural modulus of SiOC by ∼47%, reaching ∼29.9 GPa. For annealed 1% BNNT-SiOC, the flexural modulus reaches ∼47.6 GPa, representing increases of ∼133% over pyrolyzed SiOC, ∼59% over annealed SiOC, and ∼19% over pyrolyzed 1% BNNT-SiOC. A similar trend is exhibited for flexural strength. Annealed 1% BNNT-SiOC achieves a flexural strength of ∼137.4 MPa, representing a 2.5-fold increase over pyrolyzed pure SiOC (∼55.5 MPa), a 2.0-fold increase over annealed pure SiOC (∼69.3 MPa), and a ∼23% increase over pyrolyzed 1% BNNT-SiOC (∼111.6 MPa). The addition of 1% BNNTs noticeably increases the flexural strain from ∼0.27 to ∼0.33%, with this enhancement largely unaffected by thermal annealing (Table 1).

The fracture toughness of pyrolyzed SiOC is measured to be ∼0.9 MPa·m$^{1/2}$, consistent with reported literature values (∼0.6−0.84 MPa·m$^{1/2}$).[20−22] The incorporation of 1% BNNTs leads to a remarkable ∼144% increase in fracture toughness, reaching ∼2.2 MPa·m$^{1/2}$. Following thermal annealing at 1400 °C, the fracture toughness of 1% BNNT-SiOC further improves to ∼3.0 MPa·m$^{1/2}$, representing a 3.3-fold increase relative to pyrolyzed SiOC and a 2.7-fold increase compared to annealed SiOC (∼1.1 MPa·m$^{1/2}$). The substantial mechanical improvements achieved with minimal BNNT loadings underscore the exceptional potential of BNNTs as reinforcing fillers for PDCs. Moreover, our findings highlight the critical role of thermal processing conditions in governing the bulk mechanical properties of BNNT-PDC composites.

https://doi.org/10.1021/acsaenm.5c00295
ACS Appl. Eng. Mater. 2025, 3, 2383−2390

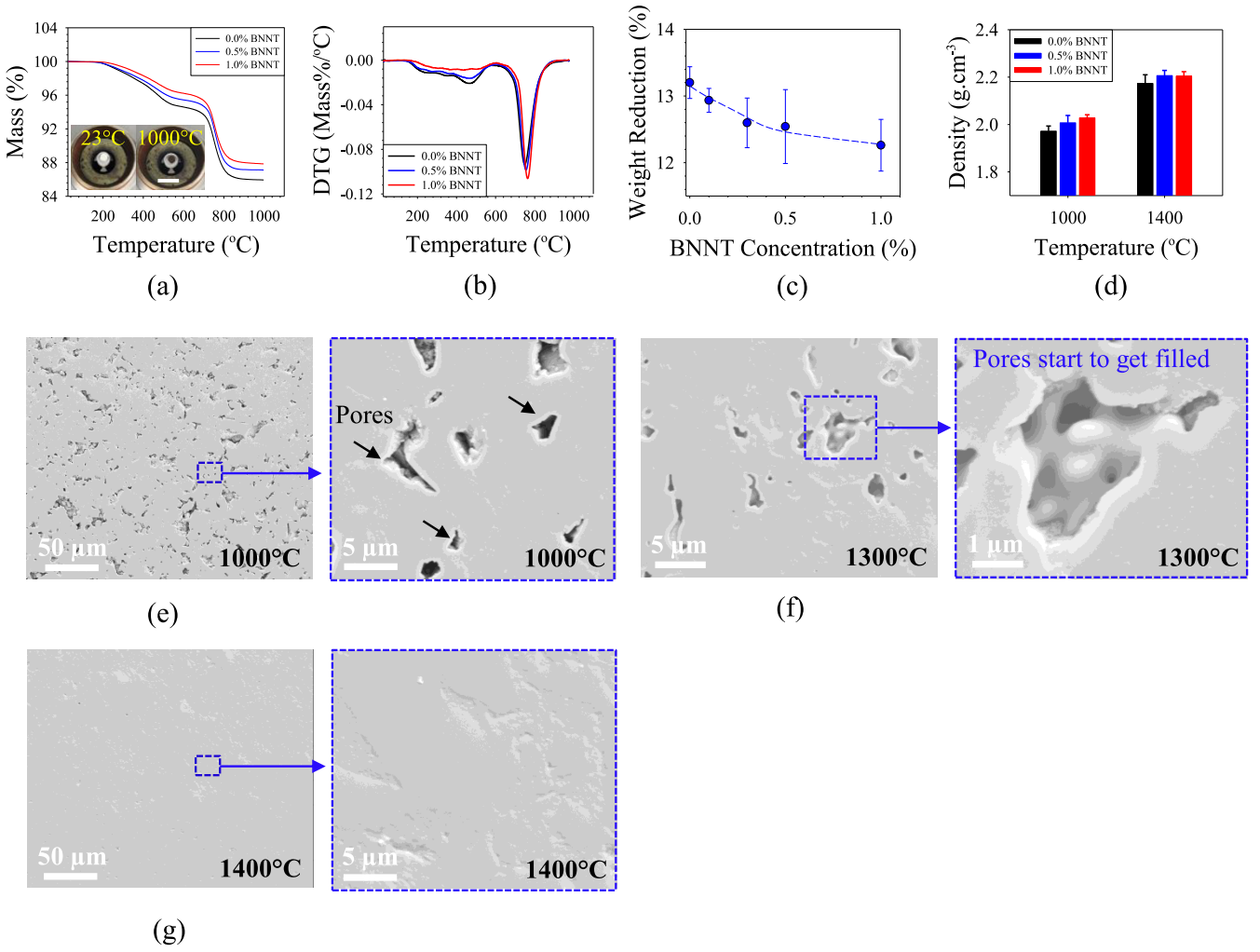

Figure 3. Thermographic analysis and microstructure characterization of BNNT-SiOC nanocomposites: (a) Measured mass change from TGA analysis (inset images: before and after heating of the sample; scale bar ~10 mm) and (b) DTG curves; (c) Measured weight change at 1000 °C; (d) Measured density after sintering at 1000 and 1400 °C; (e-g) SEM images of 0.5% BNNT-SiOC pyrolyzed at 1000 °C (e); annealed at 1300 °C (f) and 1400 °C (g).

As shown in Figure 2a, load-induced microcracks are bridged by protruding BNNTs in a fractured BNNT-SiOC specimen, revealing the primary reinforcement mechanisms at play. Individual BNNTs protruding from the fractured surface due to nanotube pullout highlight their thermal stability and efficient load transfer with the PDC matrix.[11] The bridging nanotubes inhibit crack propagation by physically spanning microcracks and facilitate energy dissipation through frictional sliding during pullout. Those microscopic features exhibit the active strengthening and toughening roles of BNNTs within the PDC matrix.

Figure 2b shows the surface morphology of fractured specimens, including pyrolyzed SiOC and both pyrolyzed and annealed 1% BNNT-SiOC. The fracture surface of SiOC is predominantly flat, exhibiting minimal plastic deformations, typical of brittle fracture behavior. In contrast, the fracture surface of pyrolyzed 1% BNNT-SiOC displays noticeable shear bands, particularly near the specimen edge. These features become more pronounced in the annealed 1% BNNT-SiOC, with shear bands extending across a larger portion of the fractured surface, indicating significant localized plastic deformations. Similar behaviors are observed in the annealed 0.5% BNNT-SiOC (Figure S4a), while the pyrolyzed counterpart exhibits no such features (Figure S4b). The observation suggests that even small additions of BNNTs can induce a marked brittle-to-ductile transition in PDCs, with the extent of this transition strongly influenced by thermal processing conditions. The improved deformability imparted by BNNTs is consistent with the increase in flexural strain (Figure 1g).

3.2. Thermographic Analysis and Microstructure Characterization

Figure 3a,b present the TGA and the corresponding derivative thermogravimetry (DTG) curves for pure cross-linked H44 and the ones with 0.5 and 1% BNNTs. All samples begin to lose weight around 200 °C, followed by a sharp decline between 700 and 900 °C, attributed to the evaporation of moisture and the release of organic functional groups, such as CH_4 and C_6H_6.[23] The organic-to-inorganic transformation continues up to 900 °C, beyond which no significant weight loss is observed. The weight loss decreases with increasing BNNT loading (Figure 3c). The observation that BNNT addition reduces weight loss can be attributed to the constraining effect of BNNTs on carbon oxidation and/or the trapping of hydrocarbon molecules near BNNT nucleation sites.[13]

https://doi.org/10.1021/acsaenm.5c00295
ACS Appl. Eng. Mater. 2025, 3, 2383−2390

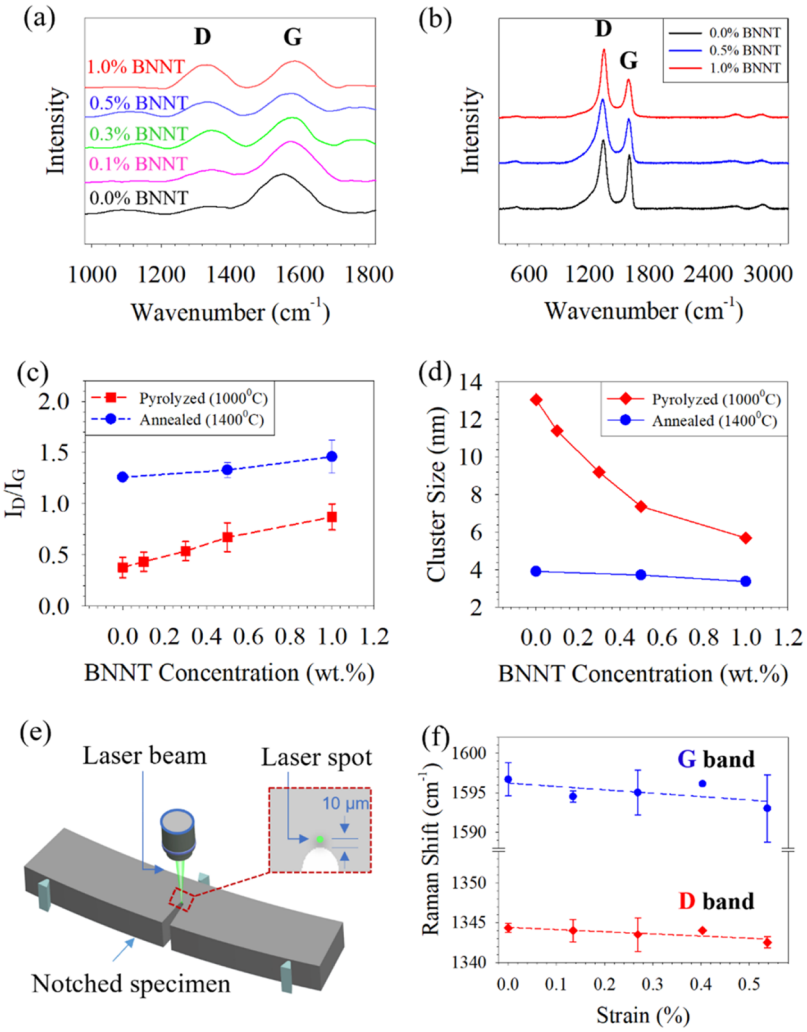

Figure 4. Raman characterization of BNNT-SiOC nanocomposites: Typical Raman spectra for (a) pyrolyzed and (b) annealed specimens; (c) The intensity ratio of the D and G bands; (d) Measured cluster size of free carbon; (e) Schematic of *in situ* Raman micromechanical characterization of a notched specimen; (f) Load-induced Raman peak shifts of the D and G bands for an annealed 1% BNNT specimen. The strain is calculated using finite element simulations (see Figure S5).

The reduced weight loss corresponds to an increase in density, as shown in Figure 3d. The density measurements were conducted for at least six different specimens of each type. The pyrolyzed 1% BNNT-SiOC exhibits a density of ~2.03 g/cm^3, noticeably higher than that of pure SiOC (~1.97 g/cm^3). After thermal annealing at 1400 °C, the density increases to ~2.17 g/cm^3 for pure SiOC and ~2.20 g/cm^3 for BNNT-SiOC, indicating a notable densification due to postpyrolyzed thermal treatment. Figure 3e–g show the porosity evolution for a pyrolyzed 0.5% BNNT-SiOC specimen annealed at different temperatures. Signs of pore filling are exhibited after annealing at 1300 °C (Figure 3f). The surface appears nearly pore-free after annealing at 1400 °C (Figure 3g), suggesting significant matrix densification and reduced matrix porosity. The increased density and reduced porosity contribute to the enhanced bulk mechanical properties by improving interfacial contact between nanotubes and the matrix, and mitigating the crack initiation.

Free carbon in pyrolyzed PDC exists in sp^2-hybridized carbon–carbon bonds, as found in graphene or carbon nanotubes.[24] This is evidenced by Raman spectroscopy through disorder-induced D bands at ~1355 cm^{-1} and a graphitic G band at ~1582 cm^{-1}. The free carbon's strong Raman signal overshadows the weaker signal of BNNTs, which is characterized by a G band at ~1369 cm^{-1}.[11]

The Raman spectra of pyrolyzed SiOC in Figure 4a show that the addition of BNNTs noticeably increases the intensity of the D band, but decreases the intensity of the G band, leading to a progressive increase of the intensity ratio (I_D/I_G) from ~0.38 (0%) to ~0.87 (1%), as displayed in Figure 4c. In comparison, annealed BNNT-SiOC exhibits an increase in the intensity ratio from ~1.24 (0%) to ~1.46 (1%) (Figure 4b). Thermal annealing at 1400 °C enhances the graphitization, leading to nanodomains of graphitic carbon nanocrystallites.[25] The observation of an increasing D band intensity upon BNNT addition can be attributed to the formation of more edges in sp^2-bonded carbon structures, resulting from BNNT-induced smaller clustering of free carbon.

Free carbon atoms tend to form clusters, and the cluster diameter (L_a) can be determined using the Tuinstra-Koenig Equation,[26] which is given as

$$L_a = \frac{C(\lambda)}{I_D/I_G} \quad (1)$$

https://doi.org/10.1021/acsaenm.5c00295
ACS Appl. Eng. Mater. 2025, 3, 2383–2390

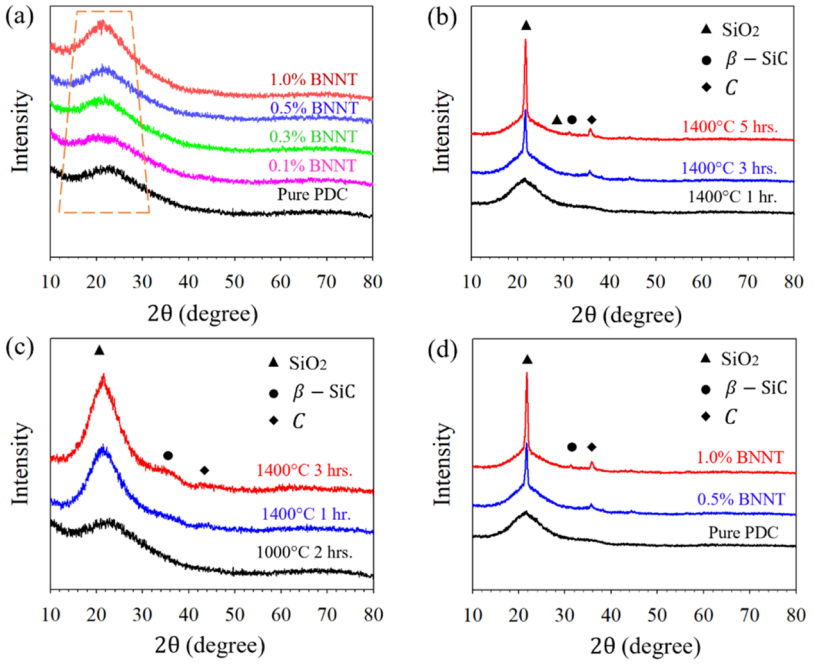

Figure 5. XRD characterization of BNNT-SiOC nanocomposites: (a) Specimens pyrolyzed at 1000 °C; (b) 0.5% BNNT specimens annealed at 1400 °C with varying hold times; (c) Pure PDC at selected sintering temperatures and holding times; (d) Comparison of spectra of annealed specimens.

where $C(\lambda) = C_0 + \lambda C_1$, in which C_0 = 12.6 nm; C_1 = 0.033; λ is the used laser wavelength (532 nm). Figure 4d shows that the cluster size of free carbon in BNNT-SiOC substantially decreases with an increase in BNNT concentration, which can be attributed to the role of BNNTs as nucleating sites for carbon clusters.[13] The influence of BNNTs on cluster size is more pronounced in pyrolyzed specimens compared to annealed specimens. Notably, adding 1% BNNTs decreases the free carbon cluster size from ∼13.1 to ∼5.7 nm for pyrolyzed BNNT-SiOC and from ∼3.9 to ∼3.4 nm for annealed BNNT-SiOC. This can be attributed to the reduction in cluster size caused by the elevated temperature during annealing. As a result, the significance of BNNTs in further reducing the cluster size is diminished compared to their effect in the pyrolyzed specimen.

Furthermore, we investigate the local load-bearing behavior of carbon nanodomains in BNNT-SiOC using *in situ* Raman micromechanical characterization techniques,[18] as illustrated in Figure 4e. The Raman measurements of an annealed, notched 1% BNNT-SiOC specimen under three-point bending reveal prominent Raman peak shifts for both the D and G bands at a location about 10 μm away from the notch tip (Figure 4f). The results indicate that the local sp^2 bonds in the carbon nanodomain are mechanically stretched in response to the global deformation of the specimen. The measured Raman peak shift per 1% matrix strain (∼-4.3 cm^{-1} for G-band and ∼−2.7 cm^{-1} for D-band) is substantially lower than the reported literature values for graphene (∼−8 to −14 cm^{-1} for G-band2[27,28] and ∼−4.7 cm^{-1} for D-band[29]). The results indicate that load transfer occurs between carbon nanodomains and the SiOC matrix; however, the actual straining of carbon nanodomains is substantially lower than that of the local matrix. It is likely attributed to the small size of the carbon nanodomain that allows at most a modest interfacial load transfer.[10,11] Nonetheless, the findings of load transfer suggest that the presence of these tiny carbon nanodomains contributes to enhancing the bulk mechanical properties of the PDC composite.

Figure 5a displays XRD results obtained from pyrolyzed BNNT-SiOC, showcasing characteristic spectra indicative of the amorphous nature of the specimens. Figure 5b presents XRD results of annealed 0.5% BNNT-SiOC with varying holding times. Sharp peaks are exhibited at 2θ∼21.9°, 35°, 44° respectively, with peak at 2θ∼21.9° being the most prominent and corresponding to the [101] plane for SiO_2.[30] The intensity of this particular peak increases with the holding time from 1 to 3 h, remaining relatively stable with a holding time of 5 h. Figure 5c illustrates XRD spectra for pure SiOC under three conditions: pyrolyzed at 1000 °C and annealed at 1400 °C with two different hold times. Higher-intensity peaks, indicative of improved SiO_2 crystallinity, are observed with increasing temperature and holding time. The comparison of the XRD results for annealed specimens in Figure 5d reveals that the intensity of the SiO_2 peak increases with increasing BNNT loading. The increase in matrix crystallinity can be attributed to both high-temperature annealing and the nucleation role of BNNTs,[31,32] enhancing the bulk mechanical properties of BNNT-SiOC. When widely distributed in the matrix, the low frictional properties of the graphitic sp^2 carbon structure facilitate sliding between adjacent phases, enhancing the bulk deformability and ductility.

4. CONCLUSIONS

This study demonstrates that adding small amounts of BNNTs significantly improves the bulk mechanical properties of polymer-derived SiOC. The enhancements are attributed to efficient load transfer at the nanotube−matrix interface and BNNT-induced favorable microstructural modifications of the matrix. The tiny sp^2-bonded carbon nanodomains from the graphitization of free carbon behave as loading-bearing elements, contributing to the strengthening of the composite. Overall, the results highlight the potential of BNNTs as

https://doi.org/10.1021/acsaenm.5c00295
ACS Appl. Eng. Mater. 2025, 3, 2383−2390

effective reinforcing fillers in PDCs, opening new avenues for developing lightweight, high-strength, tough, and durable ceramic materials.

■ ASSOCIATED CONTENT

Supporting Information

The Supporting Information is available free of charge at https://pubs.acs.org/doi/10.1021/acsaenm.5c00295.

Additional details about the mechanical and material characterization and analysis (PDF)

■ AUTHOR INFORMATION

Corresponding Author

Changhong Ke − *Department of Mechanical Engineering, State University of New York at Binghamton, Binghamton, New York 13902, United States; Materials Science and Engineering Program, State University of New York at Binghamton, Binghamton, New York 13902, United States;* orcid.org/0000-0002-5170-9859; Email: cke@binghamton.edu

Authors

Nasim Anjum − *Department of Mechanical Engineering, State University of New York at Binghamton, Binghamton, New York 13902, United States*

Dingli Wang − *Department of Mechanical Engineering, State University of New York at Binghamton, Binghamton, New York 13902, United States*

Complete contact information is available at: https://pubs.acs.org/10.1021/acsaenm.5c00295

Notes

The authors declare no competing financial interest.

■ ACKNOWLEDGMENTS

The authors gratefully acknowledge the support of the National Science Foundation under Grant Nos. CMMI 2009134 and 2425706, and DMR-2406763, and the support of the SUNY System Administration through the SUNY Research Seed Grant Award #241008.

■ REFERENCES

(1) Lacelle, T.; Sampson, K. L.; Yazdani Sarvestani, H.; Rahimizadeh, A.; Barroeta Robles, J.; Mirkhalaf, M.; Rafiee, M.; Jakubinek, M. B.; Paquet, C.; Ashrafi, B. Additive Manufacturing of Polymer Derived Ceramics: Materials, Methods, and Applications. *APL Mater.* **2023**, *11* (7), No. 070602.

(2) Sellappan, P.; Guin, J. P.; Rocherulle, J.; Celarie, F.; Rouxel, T.; Riedel, R. Influence of Diamond Particles Content on the Critical Load for Crack Initiation and Fracture Toughness of SiOC Glass-Diamond Composites. *J. Eur. Ceram. Soc.* **2013**, *33* (4), 847−858.

(3) O'Masta, M. R.; Stonkevitch, E.; Porter, K. A.; Bui, P. P.; Eckel, Z. C.; Schaedler, T. A. Additive Manufacturing of Polymer-Derived Ceramic Matrix Composites. *J. Am. Ceram. Soc.* **2020**, *103* (12), 6712−6723.

(4) Treacy, M. M. J.; Ebbesen, T. W.; Gibson, J. M. Exceptionally High Young's Modulus Observed for Individual Carbon Nanotubes. *Nature* **1996**, *381* (6584), 678−680.

(5) Wei, X.; Wang, M.-S.; Bando, Y.; Golberg, D. Tensile Tests on Individual Multi-Walled Boron Nitride Nanotubes. *Adv. Mater.* **2010**, *22* (43), 4895−4899.

(6) Jiang, Y.; Li, N.; Liu, Z.; Yi, C.; Zhou, H.; Park, C.; Fay, C. C.; Deng, J.; Chew, H. B.; Ke, C. Exceptionally Strong Boron Nitride Nanotube Aluminum Composite Interfaces. *Extreme Mech. Lett.* **2023**, *59*, No. 101952.

(7) Chen, X.; Dmuchowski, C. M.; Park, C.; Fay, C. C.; Ke, C. Quantitative Characterization of Structural and Mechanical Properties of Boron Nitride Nanotubes in High Temperature Environments. *Sci. Rep.* **2017**, *7* (1), No. 11388.

(8) Tank, M. J.; Reyes, A. N.; Park, J. G.; Scammell, L. R.; Smith, M. W.; De Leon, A.; Sweat, R. D. Extreme Thermal Stability and Dissociation Mechanisms of Purified Boron Nitride Nanotubes: Implications for High-Temperature Nanocomposites. *ACS Appl. Nano Mater.* **2022**, *5* (9), 12444−12453.

(9) Li, N.; Dmuchowski, C. M.; Jiang, Y.; Yi, C.; Gou, F.; Deng, J.; Ke, C.; Chew, H. B. Sliding Energy Landscape Governs Interfacial Failure of Nanotube-Reinforced Ceramic Nanocomposites. *Scr. Mater.* **2022**, *210*, No. 114413.

(10) Yi, C.; Bagchi, S.; Gou, F.; Dmuchowski, C. M.; Park, C.; Fay, C. C.; Chew, H. B.; Ke, C. Direct Nanomechanical Measurements of Boron Nitride Nanotube—Ceramic Interfaces. *Nanotechnology* **2019**, *30* (2), No. 025706.

(11) Anjum, N.; Wang, D.; Gou, F.; Ke, C. Boron Nitride Nanotubes Toughen Silica Ceramics. *ACS Appl. Eng. Mater.* **2024**, *2* (3), 735−746.

(12) Du, M.; Bi, J.-Q.; Wang, W.-L.; Sun, X.-L.; Long, N.-N. Microstructure and Properties of SiO2Matrix Reinforced by BN Nanotubes and Nanoparticles. *J. Alloys Compd.* **2011**, *509* (41), 9996−10002.

(13) Jia, Y.; Ajayi, T. D.; Morales, J.; Chowdhury, M. A. R.; Sauti, G.; Chu, S. H.; Park, C.; Xu, C. Thermal Properties of Polymer-Derived Ceramic Reinforced with Boron Nitride Nanotubes. *J. Am. Ceram. Soc.* **2019**, *102* (12), 7584−7593.

(14) Li, H.; Shahriari, L.; Khandwani, Y.; Talevich, S.; Reyes, A.; Sweat, R.; Mao, K.; Scammell, L. R.; Whitney, R. R.; Park, J. G.; Wu, Q.; Liang, Z.; Yu, Z. Polymer-Derived Silicon Carbide and Boron Nitride Nanotube Composites with High Thermal Shock Resistance. *ACS Appl. Eng. Mater.* **2023**, *1* (12), 3205−3213.

(15) Smith, M. W.; Jordan, K. C.; Park, C.; Kim, J.-W.; Lillehei, P. T.; Crooks, R.; Harrison, J. S. Very Long Single- and Few-Walled Boron Nitride Nanotubes via the Pressurized Vapor/Condenser Method. *Nanotechnology* **2009**, *20* (50), No. 505604.

(16) Yamakov, V.; Park, C.; Kang, J. H.; Chen, X.; Ke, C.; Fay, C. Piezoelectric and Elastic Properties of Multiwall Boron-Nitride Nanotubes and Their Fibers: A Molecular Dynamics Study. *Comput. Mater. Sci.* **2017**, *135*, 29−42.

(17) Chen, X.; Zhang, L.; Park, C.; Fay, C. C.; Wang, X.; Ke, C. Mechanical Strength of Boron Nitride Nanotube-Polymer Interfaces. *Appl. Phys. Lett.* **2015**, *107* (25), No. 253105.

(18) Wang, D.; Chen, R.; Anjum, N.; Ke, C. Thermal Expansion of Boron Nitride Nanotubes and Additively Manufactured Ceramic Nanocomposites. *Nanotechnology* **2025**, *36* (6), No. 065703.

(19) Mera, G.; Tamayo, A.; Nguyen, H.; Sen, S.; Riedel, R. Nanodomain Structure of Carbon-Rich Silicon Carbonitride Polymer-Derived Ceramics. *J. Am. Ceram. Soc.* **2010**, *93* (4), 1169−1175.

(20) Yu, M.; Picot, O. T.; Saunders, T. G.; Dlouhý, I.; Feng, J.; Titirici, M. M.; Mahajan, A.; Reece, M. J. Graphene-Reinforced Silicon Oxycarbide Composites Prepared by Phase Transfer. *Carbon* **2018**, *139*, 813−823.

(21) Sorarù, G. D.; Tavonatti, C.; Kundanati, L.; Pugno, N.; Biesuz, M. Effect of the Pyrolysis Atmosphere on the Mechanical Properties of Polymer-Derived SiOC and SiCN. *J. Am. Ceram. Soc.* **2020**, *103* (11), 6519−6530.

(22) Eom, J. H.; Kim, Y. W. Effect of Starting Particle Size and Barium Addition on Flexural Strength of Polysiloxane-Derived SiOC Ceramics. *J. Ceram. Soc. Jpn.* **2015**, *123* (1435), 142−146.

(23) Vakifahmetoglu, C.; Colombo, P. A Direct Method for the Fabrication of Macro-Porous SiOC Ceramics from Preceramic Polymers. *Adv. Eng. Mater.* **2008**, *10* (3), 256−259.

(24) Peng, Y.; Wang, K.; Yu, M.; Li, A.; Bordia, R. K. An Optimized Process for in Situ Formation of Multi-Walled Carbon Nanotubes in

Templated Pores of Polymer-Derived Silicon Oxycarbide. *Ceram. Int.* **2017**, *43* (4), 3854−3860.
(25) Wen, Q.; Yu, Z.; Riedel, R. The Fate and Role of in Situ Formed Carbon in Polymer-Derived Ceramics. *Prog. Mater. Sci.* **2020**, *109*, No. 100623.
(26) Tuinstra, F.; Koenig, J. L. Raman Spectrum of Graphite. *J. Chem. Phys.* **1970**, *53* (3), 1126−1130.
(27) Mohiuddin, T. M. G.; Lombardo, A.; Nair, R. R.; Bonetti, A.; Savini, G.; Jalil, R.; Bonini, N.; Basko, D. M.; Galiotis, C.; Marzari, N.; Novoselov, K. S.; Geim, A. K.; Ferrari, A. C. Uniaxial Strain in Graphene by Raman Spectroscopy: G Peak Splitting, Gr\"uneisen Parameters, and Sample Orientation. *Phys. Rev. B* **2009**, *79* (20), No. 205433.
(28) Tang, B.; Guoxin, Hu.; Gao, H. Raman Spectroscopic Characterization of Graphene. *Appl. Spectrosc. Rev.* **2010**, *45* (5), 369−407.
(29) Chang, C.-C.; Chen, C.-C.; Hung, W.-H.; Hsu, I.-K.; Pimenta, M. A.; Cronin, S. B. Strain-Induced D Band Observed in Carbon Nanotubes. *Nano Res.* **2012**, *5* (12), 854−862.
(30) Duan, W.; Yin, X.; Ye, F.; Li, Q.; Han, M.; Liu, X.; Cai, Y. Synthesis and EMW Absorbing Properties of Nano SiC Modified PDC-SiOC. *J. Mater. Chem. C* **2016**, *4* (25), 5962−5969.
(31) Suplicz, A.; Szabo, F.; Kovacs, J. G. Injection Molding of Ceramic Filled Polypropylene: The Effect of Thermal Conductivity and Cooling Rate on Crystallinity. *Thermochim. Acta* **2013**, *574*, 145−150.
(32) Ning, J.; Zhang, J.; Pan, Y.; Guo, J. Fabrication and Mechanical Properties of SiO2Matrix Composites Reinforced by Carbon Nanotube. *Mater. Sci. Eng., A* **2003**, *357* (1), 392−396.

https://doi.org/10.1021/acsaenm.5c00295
ACS Appl. Eng. Mater. 2025, 3, 2383−2390